Energy 159 (2018) 1206–1217

Contents lists available at ScienceDirect

Energy

journal homepage: www.elsevier.com/locate/energy

Exergy-based thermal management of a steelmaking process linked with a multi-generation power and desalination system

H. Ishaq [a, *], I. Dincer [a], G.F. Naterer [b]

[a] Faculty of Engineering and Applied Science, University of Ontario Institute of Technology, 2000 Simcoe Street North, Oshawa, Ontario, L1H 7K4, Canada
[b] Faculty of Engineering and Applied Science, Memorial University of Newfoundland, 240 Prince Phillip Drive, St. John's, Newfoundland and Labrador, A1B 3X5, Canada

ARTICLE INFO

Article history:
Received 24 May 2018
Received in revised form
27 June 2018
Accepted 28 June 2018
Available online 29 June 2018

Keywords:
Thermal management
Desalination
Hydrogen production
Multi-generation
Energy
Exergy
Efficiency

ABSTRACT

A novel multi-generation integrated energy system is presented in this paper, consisting of a gas-steam combined cycle, four-step thermochemical copper-chlorine (Cu–Cl) cycle, proton exchange membrane fuel cell (PEMFC) and a reverse osmosis (RO) desalination unit. Effective thermal management of waste heat is recognized as a key objective in the steel industry. Hydrogen, electricity, fresh water and heat are the useful outputs of the integrated system. The produced electricity supplies the electricity load required by the electrolyzer, compressor and pumps while the supplementary electricity is an additional system product. Aspen Plus and Engineering Equation Solver (EES) are used for modeling and simulation of the multi-generation system. The overall hydrogen production rate of the designed system is 51.8 kg/hr and the net power production is 1.7 MW. The overall energy efficiency of the multi-generation system is 63.3% and the exergy efficiency is 58.8%. Further sensitivity studies and outcomes are presented and discussed in this paper.

1. Introduction

Global energy demand is increasing rapidly. The majority of current worldwide energy demand is met by fossil fuels. A key drawback of fossil fuels is the emissions produced which result in various environmental problems and global warming. Hydrogen has the benefit of serving as both an effective energy carrier and a promising energy storage medium [1]. The thermochemical Cu–Cl cycle is one of the promising technologies for hydrogen production as a clean energy carrier [2–5].

Naterer et al. [6] presented recent advances on hydrogen production through the thermochemical copper-chlorine (Cu–Cl) cycle. An international research team has conducted numerical and experimental studies on the various unit operations. Experimental results based on the electrolysis process (CuCl/HCl) and system integration of the copper-chlorine (Cu–Cl) cycle were presented. A novel quaternary solubility model for copper oxychloride (Cu_2OCl_2) was presented, through which selective precipitation of cupric chloride is optimized upstream of the hydrolysis reactor. Furthermore, recent developments on photo-electrochemical cell development were reported.

Szargut [7] presented a study on the regenerative feed-water heater influence steam power plant and hydrogen production (HP) plant operational costs. The influence is determined through the incremental energy efficiency. The incremental energy efficiency refers to the ratio of electricity production increase to the fuel chemical energy consumption increase. A constant steam flow rate is assumed at the turbine outlet of the power plant or a specified heat flow rate of the HP plant.

Wang et al. [8] presented a thermal design using a solar energy source integrated with molten salt energy storage and a thermochemical copper-chlorine (Cu–Cl) cycle. Numerous operational temperature ranges of several technologies of solar thermal energy were analyzed according to their suitability with solar hydrogen production by thermochemical cycles. It was shown that 530 °C for the maximum temperature is required by the decomposition step (oxygen production) which can be achieved by existing solar thermal technologies. The design of a solar plant (absorbing and storing energy) and molten salt quantity for an industrial scale of hydrogen production were conducted on the basis of 24 h per day of operations. The molten salt intermediate product produced during the oxygen production step can link with existing solar thermal technologies. Numerous flow layouts of solar thermal technologies

* Corresponding author.
E-mail address: haris.ishaq@uoit.net (H. Ishaq).

https://doi.org/10.1016/j.energy.2018.06.213
0360-5442/

with the copper-chlorine cycle were presented and analyzed with thermal network analyses.

A study was conducted by Szargut [9] on the design optimization of non-renewable resource depletion [9]. A formulation of a thermo-ecological objective function was presented in the study. By optimizing heat exchanger parameters, an objective function and detailed formulation were established. The model specifies the influence and difficulties in the design parameters on the fabrication process.

Liang et al. [10] presented a method for membrane electrode assembly preparation in a proton exchange membrane fuel cell (PEMFC). For membrane electrode assembly, a low interfacial resistance is a reason behind the effectiveness of the decal transfer method. In the paper, a modified decal method is presented which can achieve complete decal transfer. The optimization of the transfer pressure, drying process and catalyst inks was also considered in this study. Furthermore, numerous samples of membrane electrode assembly catalyst layers were tested for the PEMFC application.

Szargut and Szczygiel [11] conducted a comparison of primary gas turbine alternatives in terms of the efficiency accompanying a coal-fire based power plant. Four variants of a primary gas turbine installation complementing a coal-fire based power plant are considered with respect to their thermodynamic effects. These variants differ in heat recovery utilization modes of a gas turbine. The heat flows can be utilized for steam power plant water preheating and also for secondary steam superheating. An additional gas turbine expands the compressed gas down to a lower pressure coupled with a supplementary compressor. Exergy loss reduction in the boiler heat recovery was a key objective in the system design.

Gantenberg et al. [12] presented a study on heat recovery from water and gas and their effects on the blast furnace operating expenditures. It was observed that with an increase in energy prices, the price of gases with a high calorific value increased drastically. Hot blast stoves allow the energy in the stove plant waste gas to be recovered. Energy recovered is utilized for combustion air preheating. Heat recovery by the waste gas leads to less overall gas consumption by replacing gas through the blast furnace to gas which results in a reduction of blast furnace operational expenditures. Energy available for preheating is enhanced by auxiliary burners to improve the heat utilization. A feasibility evaluation of gas consumption was studied in the paper to reduce the operational expenditures.

Si [13] reported the waste heat recovery feasibility in a steel plant and its effect on the energy efficiency assessment. Numerous energy efficiency assessment opportunities were considered at a Gerdau Manitoba Mill in Manitoba, Canada, including upgrades of a reheat furnace; natural gas heaters replaced by indirect-fire heaters; preheat billets via waste heat recovery; waste heat recovery for preheating combustion air; and oxyfuel combustion. This study revealed that a bottom tapping furnace was the major consumer of electricity. The reduction of the downtime in the bottom tapping furnace at the Gerdau Manitoba mill was also analyzed. Flue gas losses caused by the reheat furnace were major energy losses in the system. During operation, roof and hearth heat losses accounted for 8.9% of energy losses.

A study based on liquid natural gas cryogenic exergy usage for electricity production was presented by Szargut and Szczygiel [14]. Compressed liquid natural gas is transported through sea-ships and evaporated before flowing in system pipelines. The processes of cryogenic exergy usage carried by liquid natural gas were analyzed for production of electricity without involving any additional combustion. Three different plant cases were investigated in the study. A cascade system containing two working fluids was analyzed. It was shown that the optimum temperature difference is higher than primarily assumed in liquid natural gas. Thus, a third variant containing a single working fluid, ethane, was also analyzed in this study. The produced electricity, pay-back and annual profit were evaluated as well. Another related study [15] was conducted on the ambient temperature effects on the gas turbine operating conditions.

Thermal management of steel furnace waste heat is considered in this paper. The proposed system consists of a gas-steam combined cycle, thermochemical copper-chlorine (Cu–Cl) cycle, proton exchange membrane fuel cell and a reverse osmosis desalination unit. The system is based on multi-generation outputs of hydrogen, electricity, fresh water and heat. Oxygen produced by the decomposition reaction and partial amount of hydrogen produced from the electrolysis step are utilized in a PEM fuel cell to produce electricity and heat. The primary objective of this paper is to develop and exergetically examine a novel thermal management option for an industrial steelmaking process. The heat recovered from the process is utilized to produce hydrogen and oxygen via a thermochemical copper-chlorine (Cu–Cl) cycle. The oxygen and a partial amount of hydrogen are used in a PEM fuel cell for electricity and heat production while additional heat available in the condenser is used in an RO desalination unit. The proposed analysis aims to recover additional heat throughout the system and utilize it for producing useful products. The paper also aims to improve the energy and exergy efficiencies of the system.

2. System description

The input heat source for the proposed multi-generation system is the exhaust gas released from a steel melting furnace. The system has four major outputs of hydrogen, electricity, fresh water and heat. The major subsystems of the proposed system are a combined power cycle, thermochemical copper-chlorine (Cu–Cl) cycle, reverse osmosis desalination unit and proton exchange membrane fuel cell. Fig. 1 shows a schematic diagram of the system. The system consists of the following major subsystems.

2.1. Combined gas-steam power cycle

Flue gas from a steel melting furnace is utilized to produce useful products. Consider a typical steel furnace with a flue gas ejected from the furnace at a temperature of 810 °C and mass flow rate of 9.2 kg/s. This flue gas is initially passed through a heat exchanger where it transfers heat to the water stream which is flowing towards the thermochemical Cu–Cl cycle and the remaining heat flows to the third air stream. An air stream enters the heat exchanger B1 via stream S10, absorbs heat from the heat exchanger and leaves through stream S7 at a high temperature. This stream then enters the gas turbine B3. In the gas turbine, compressed air expands, produces the electricity and flows towards the heat exchanger B4. This heat exchanger works as a boiler for the Rankine cycle combined with a gas power cycle. From the heat exchanger B4, stream flows towards the compressor B5 which compresses the air at a high pressure and re-circulates the air into heat exchanger B1.

Various parameters of the system are shown in Table 2. A stream B14 containing water arrives at the heat exchanger B4 at a high pressure where heat is transferred between S8 and S14 streams and water is vaporized into superheated steam. This superheated steam reaches the steam turbine B6 at a high temperature and pressure. Electricity is generated the through the steam turbine by expanding this superheated steam. The exit stream from the turbine arrives at the condenser B7 via the S12 stream. At this point, this stream maintains thermal energy which is utilized for the reverse osmosis desalination unit. The stream S13 then enters the pump B8 which

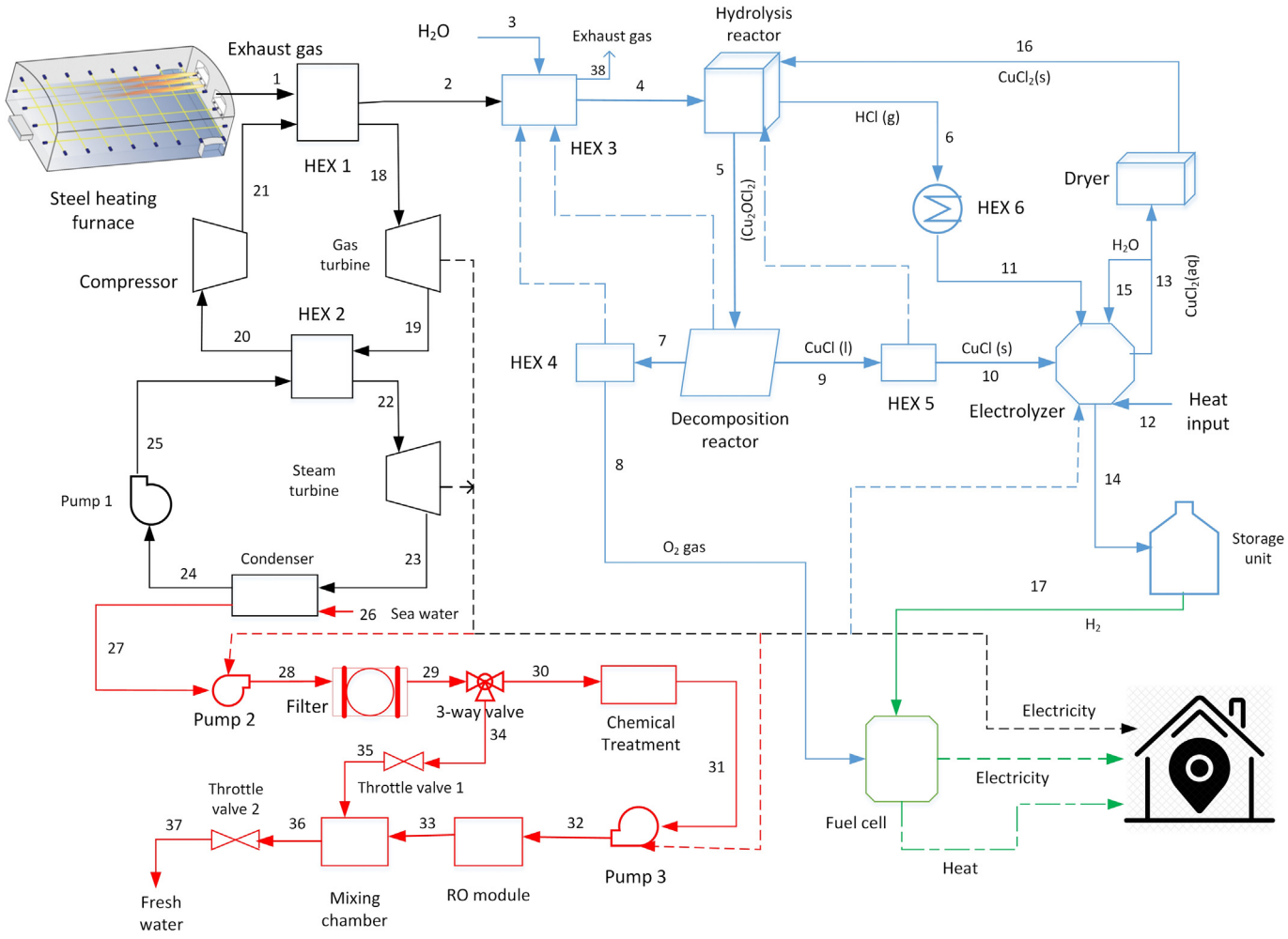

Fig. 1. Schematic diagram of the system consisting of a gas-steam combined cycle, Cu–Cl cycle, PEM fuel cell and RO desalination unit.

increases its temperature and re-circulates the water towards heat exchanger B4. This gas-steam combined cycle remains in continuous operation. Fig. 2 shows the Aspen Plus model of the gas-steam combined cycle.

2.2. Water splitting Cu–Cl cycle

A water splitting copper-chlorine (Cu–Cl) cycle is the hydrogen production method involving four major steps: hydrolysis, thermolysis, electrolysis and water separation by drying or crystallization. The reactions of all four steps are shown in Table 1.

A stream S3 containing water enters the heat exchanger B1 and leaves the heat exchanger via stream S4 after absorbing heat from the flue gas. This stream then splits into two streams S5 and S6. Stream S5 reaches the heat exchanger B10 which maintains its temperature and this stream further enters the hydrolysis reactor B12 through the S15 stream. Another stream S32 arrives at the hydrolysis reactor carrying cupric chlorine ($CuCl_2$). In the hydrolysis reactor, water reacts with $CuCl_2$ at 400 °C and produces copper oxychloride (Cu_2OCl_2) and hydrogen chloride (HCl) gas. This hydrolysis reactor absorbs the required amount of heat.

The mixture of copper oxychloride and hydrogen chloride gas is separated through a B13 separator via S17 and S18 streams. The stream S17 arrives at the heat exchanger B14 and maintains its temperature at 500 °C. The exit stream from the heat exchangers reaches the decomposition reactor B16. Another stream S6 which splits through the B2 splitter arrives at the heat exchanger B11 and then reaches the decomposition reactor. This decomposition reactor decomposes cuprous chloride (CuCl) and oxygen gas at 500 °C which are separated through the B17 separator. This oxygen gas is used in a proton exchanger membrane fuel cell for electricity production while CuCl enters the heat exchanger B18 where additional heat is recovered from CuCl. Another stream S18 containing HCl enters the heat exchanger B15 where additional heat is recovered and then HCl reaches the electrolysis reactor B19.

In the electrolysis reactor, cuprous chloride reacts with hydrogen chloride in an aqueous solution and produces cupric chloride $CuCl_2$ and hydrogen gas. A part of this hydrogen gas is used in a proton exchanger membrane fuel cell for electricity and heat production. Hydrogen gas is separated from aqueous $CuCl_2$ through the B20 separator. Aqueous cupric chloride then arrives at the dryer B22 which separates the water from cupric chloride and re-cycles this $CuCl_2$ into the hydrolysis reactor in order to continue the process.

The overall copper-chlorine cycle contains only one input of water and two outputs of hydrogen and oxygen while all remaining compounds are recycled throughout the process. Fig. 3 shows the Aspen Plus layout of the thermochemical Cu–Cl cycle.

2.3. Proton exchange membrane (PEM) fuel cell

A proton exchange membrane (PEM) fuel cell is advantageous

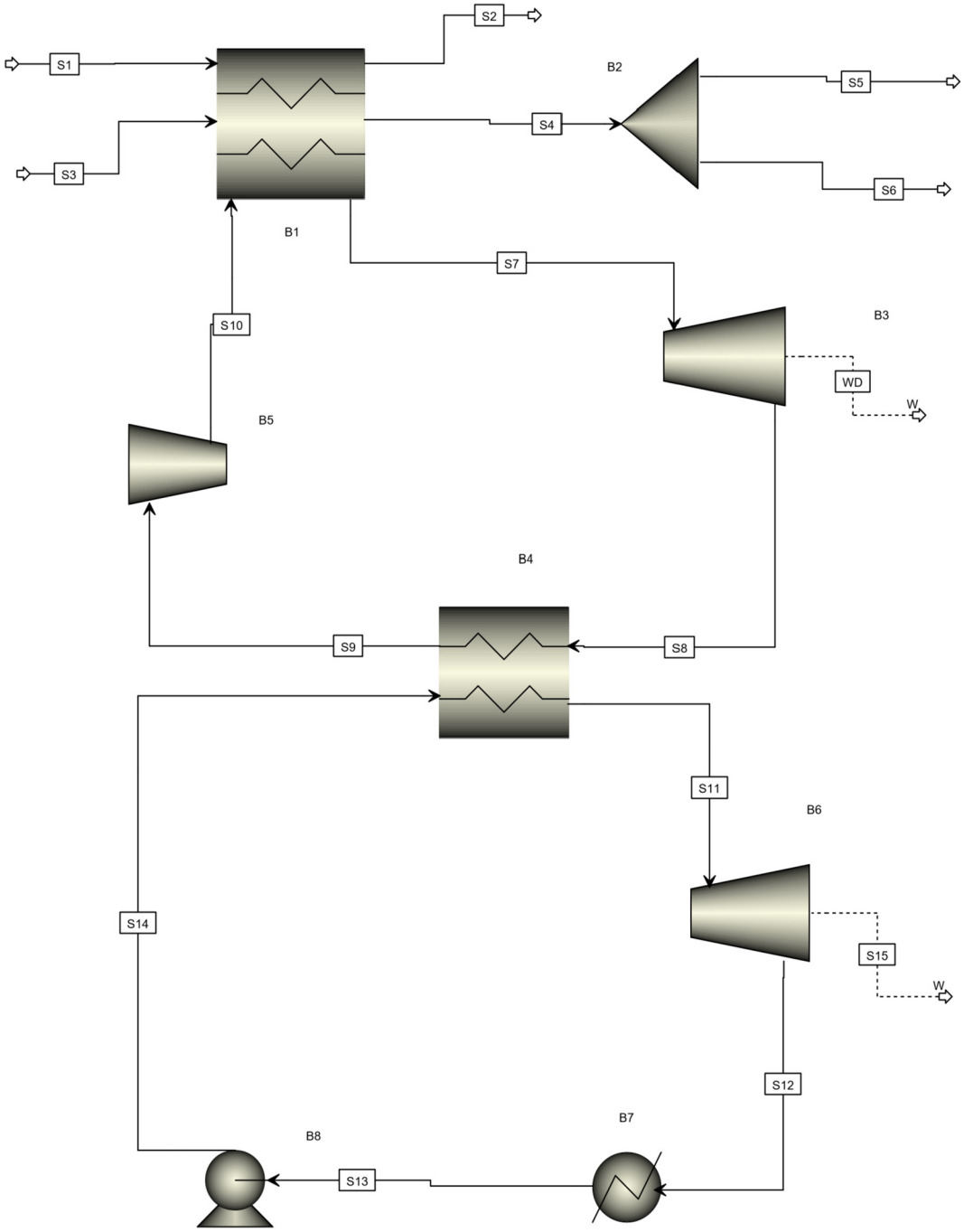

Fig. 2. Aspen Plus layout of gas-steam combined cycle.

Table 1
Four-step copper-chlorine cycle [16].

Step	Reaction	Temperature range (°C)	Step name
1	$2CuCl(aq) + 2HCl(aq) \rightarrow H_2(g) + 2CuCl_2(aq)$	<100	Hydrogen production
2	$CuCl_2(aq) \rightarrow CuCl_2(s)$	<100	Drying
3	$2CuCl_2(s) + H_2O(g) \rightarrow Cu_2OCl_2(s) + 2HCl(g)$	400	Hydrolysis
4	$Cu_2OCl_2(s) \rightarrow 0.5O_2(g) + 2CuCl(l)$	500	Thermolysis

over other types because of its comparatively low operating temperature of around 80 °C, quick start-up, high power density and relatively low emission of nitrogen and sulfur oxides. In PEM fuel cells, an ion exchange membrane is used with the electrolyte. In a PEM fuel cell, the output of heat and electricity increase with an increase in temperature, and they decrease with an increase in

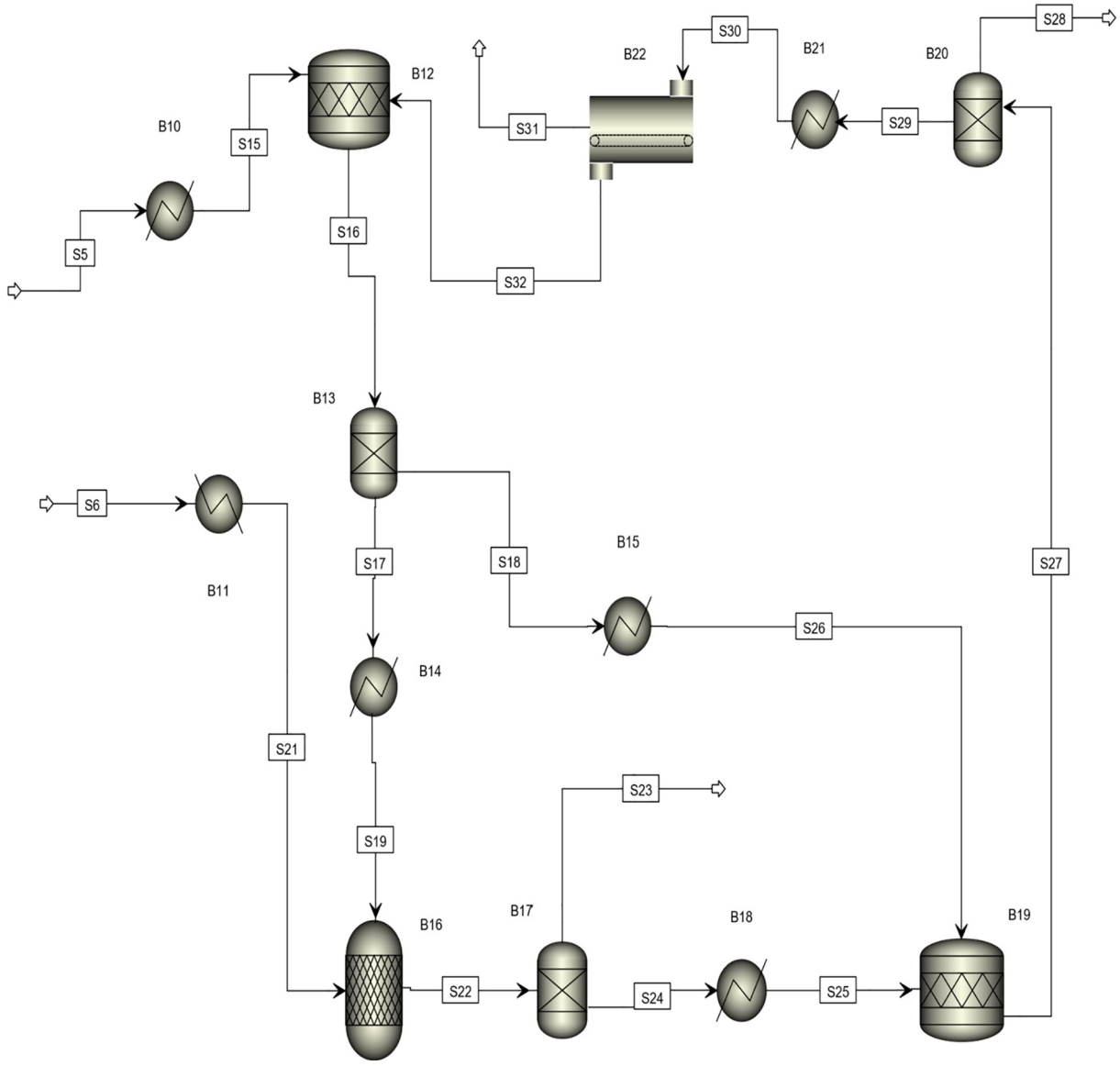

Fig. 3. Aspen Plus flowsheet of water splitting copper-chlorine cycle.

membrane thickness. Oxygen gas produced by the decomposition reactor reacts with hydrogen gas in the PEM fuel cell and produces heat and electricity. Typical operating and design parameters of PEM fuel cell are shown in Table 3.

The anodic and cathodic reactions of the fuel cell respectively are given as follows:

Table 2
Significant parameters of system [17].

Parameter	Value
Flue gas input temperature	810 °C
Mass flow rate of flue gas	9.2 kg/s
S4 stream temperature leading to Cu–Cl cycle	550 °C
Discharge pressure of gas turbine B3	1 bar
Rankine cycle operating pressure	5 MPa
Discharge pressure of steam turbine B6	0.1 bar
Hydrolysis reactor B12 temperature	400 °C
Decomposition reactor B16 temperature	500 °C
Electrolysis reactor B19 temperature	25 °C
Electrical energy requirement by electrolysis reactor B19	55.0 kJ/mol H_2
Dryer B22 temperature	80 °C

Table 3
Operating parameters of PEM fuel cell [18].

Parameter	Range	Unit
Current density of fuel cell	11,500	A/m^2
Cell operating temperature	80	°C
Cell area	1	m^2
Operating pressure of fuel cell	100	kPa
Fuel cell heat rate	1518	W

$$H_2 \rightarrow 2H^+ + 2e^- \quad (1)$$

$$\frac{1}{2}O_2 + 2H^+ + 2e^- \rightarrow H_2O \quad (2)$$

2.4. Reverse osmosis (RO) desalination unit

Heat flow from the condenser in utilized to produce fresh water through a reverse osmosis desalination unit. Fresh water enters at room temperature and leaves at 45 °C after absorbing heat from the

Table 4
Significant parameters of RO desalination unit [19].

Parameter	Value
Salinity of sea water	35,000 ppm
Salinity of product water	450 ppm
Fresh water flow rate	2.3 kg/s
Sea water temperature	25 °C
Pump efficiency	85%
Membrane recovery ratio	60%

condenser. A schematic diagram of a reverse osmosis desalination unit is shown in Fig. 1. Engineering Equation Solver (EES) is the software used for analysis of the RO desalination unit. The operating and design parameters of the RO desalination unit are shown in Table 4. Heated water first reaches the low pressure pump which operates at 650 kPa and increases the water pressure. Water then reaches the filter where suspended particles are removed via filters. Then it flows towards a valve which separates the water in a separate stream before it arrives at a chemical treatment step. Then it reaches a high pressure pump which increases the water pressure up to 6000 kPa. From the high pressure turbine, water flow towards a reverse osmosis (RO) module and mixing chamber. At the last step, fresh water is separated by passing it through a second throttle valve.

3. System analysis and assessment

For all components, steady state operating conditions are assumed [17]. All gases are treated as real gases. Kinetic and gravitational energy changes are neglected [20]. An isentropic efficiency of 72% is assumed for the compressor [21]. SOLID in the property method is used in Aspen Plus [22]. The electrical generator efficiency is assumed as 95% [23]. An isentropic efficiency of 72% is assumed for all turbines [21]. Pressure drops and heat losses are neglected in heat exchangers [24]. The sea water salinity is assumed to be 35,000 PPM [25].

Aspen Plus and Engineering Equation Solver are used for the modeling and simulation. Aspen Plus flowsheets are shown in Figs. 2 and 3. In Aspen Plus software, the SOLID property is used. The major subsystems are the gas-steam combined cycle, thermochemical copper-chlorine cycle, proton exchange membrane fuel cell (PEMFC) and Reverse Osmosis (RO) desalination unit. The system contains four major outputs of hydrogen, electricity, fresh water and heat. On the basis of a thermodynamic analysis, the energy, entropy, and exergy balance equations of all major components are shown in Table 5. The exergy efficiencies of all components are shown in Table 6.

The general balance equations of mass, energy, entropy and exergy are written as follows [26,27]:

- General mass balance equation:

$$\sum_{i}\dot{m}_i = \sum_{e}\dot{m}_e \tag{3}$$

- General energy balance equation:

$$\dot{Q}_i + \dot{W}_i + \sum_{i}\dot{m}_i\left(h_i + \frac{V_i^2}{2} + gZ_i\right) = \dot{Q}_e + \dot{W}_e + \sum_{e}\dot{m}_e\left(h_e + \frac{V_e^2}{2} + gZ_e\right) \tag{4}$$

- General entropy balance equation:

Table 5
Energy and exergy balance equations of major components of the system.

Component	Energy balance equation	Exergy balance equation
B1 (heat exchanger)	$\dot{m}_{s1}h_{s1} + \dot{m}_{s3}h_{s3} + \dot{m}_{s10}h_{s10} = \dot{m}_{s2}h_{s2} + \dot{m}_{s4}h_{s4} + \dot{m}_{s7}h_{s7}$	$\dot{m}_{s1}ex_{s1} + \dot{m}_{s3}ex_{s3} + \dot{m}_{s10}ex_{s10} = \dot{m}_{s2}ex_{s2} + \dot{m}_{s4}ex_{s4} + \dot{m}_{s7}ex_{s7} + \dot{E}x_d$
B3 (Gas turbine)	$\dot{m}_{s7}h_{s7} = \dot{m}_{s8}h_{s8} + \dot{W}_{out}$	$\dot{m}_{s7}ex_{s7} = \dot{m}_{s8}ex_{s8} + \dot{W}_{out} + \dot{E}x_d$
B4 (heat exchanger)	$\dot{m}_{s8}h_{s8} + \dot{m}_{s14}h_{s14} = \dot{m}_{s9}h_{s9} + \dot{m}_{11}h_{s11}$	$\dot{m}_{s8}ex_{s8} + \dot{m}_{s14}ex_{s14} = \dot{m}_{s9}ex_{s9} = \dot{m}_{s14}ex_{s14} + \dot{E}x_d$
B5 (compressor)	$\dot{m}_{s9}h_{s9} + \dot{W}_{in} = \dot{m}_{s10}h_{s10}$	$\dot{m}_{s9}ex_{s9} + \dot{W}_{in} = \dot{m}_{s10}ex_{s10} + \dot{E}x_d$
B6 (steam turbine)	$\dot{m}_{s11}h_{s11} = \dot{m}_{s12}h_{s12} + \dot{W}_{out}$	$\dot{m}_{s11}ex_{s11} = \dot{m}_{s12}ex_{s12} + \dot{W}_{out} + \dot{E}x_d$
B8 (pump 1)	$\dot{m}_{s13}h_{s13} + \dot{W}_{in} = \dot{m}_{s14}h_{s14}$	$\dot{m}_{s13}ex_{s13} + \dot{W}_{in} = \dot{m}_{s14}ex_{s14} + \dot{E}x_d$
B10 (heat exchanger)	$\dot{m}_{s5}h_{s5} + \dot{Q}_{in} = \dot{m}_{s15}h_{s15}$	$\dot{m}_{s5}ex_{s5} + \dot{E}x_{\dot{Q}_{in}} = \dot{m}_{s15}ex_{s15} + \dot{E}x_d$
B11 (heat exchanger)	$\dot{m}_{s6}h_{s6} + \dot{Q}_{in} = \dot{m}_{s21}h_{s21}$	$\dot{m}_{s6}ex_{s6} + \dot{E}x_{\dot{Q}_{in}} = \dot{m}_{s21}ex_{s21} + \dot{E}x_d$
B12 (hydrolysis reactor)	$\dot{m}_{s15}h_{s15} + \dot{m}_{s32}h_{s32} + \dot{Q}_{in} = \dot{m}_{s16}h_{s16}$	$\dot{m}_{s15}ex_{15} + \dot{m}_{s32}ex_{32} + \dot{E}x_{\dot{Q}_{in}} = \dot{m}_{s16}ex_{s16} + \dot{E}x_d$
B13 (separator)	$\dot{m}_{s16}h_{s16} = \dot{m}_{s18}h_{s18} + \dot{m}_{s17}h_{s17}$	$\dot{m}_{s16}ex_{s16} = \dot{m}_{s18}ex_{s18} + \dot{m}_{s17}ex_{s17} + \dot{E}x_d$
B16 (decomposition reactor)	$\dot{m}_{s21}h_{s21} + \dot{m}_{s19}h_{s19} + \dot{Q}_{in} = \dot{m}_{s22}h_{s22}$	$\dot{m}_{s21}ex_{s21} + \dot{m}_{s19}ex_{s19} + \dot{E}x_{\dot{Q}_{in}} = \dot{m}_{s22}ex_{s22} + \dot{E}x_d$
B18 (heat exchanger)	$\dot{m}_{s24}h_{s24} = \dot{m}_{s25}h_{s25} + \dot{Q}_{out}$	$\dot{m}_{s24}ex_{s24} = \dot{m}_{s25}ex_{s25} + \dot{E}x_{\dot{Q}_{out}} + \dot{E}x_d$
B19 (electrolysis reactor)	$\dot{m}_{s25}h_{s25} + \dot{m}_{s26}h_{s26} + \dot{W}_e = \dot{m}_{s27}h_{s27}$	$\dot{m}_{s25}ex_{s25} + \dot{m}_{s26}ex_{s26} + \dot{W}_e = \dot{m}_{s27}ex_{s27} + \dot{E}x_d$
B20 (separator)	$\dot{m}_{s27}h_{s27} = \dot{m}_{s28}h_{s28} + \dot{m}_{s29}h_{s29}$	$\dot{m}_{s27}ex_{s27} = \dot{m}_{s28}ex_{s28} + \dot{m}_{s29}ex_{s29} + \dot{E}x_d$
B21 (heat exchanger)	$\dot{m}_{s29}h_{s29} + \dot{Q}_{in} = \dot{m}_{s30}h_{s30}$	$\dot{m}_{s29}ex_{s29} + \dot{E}x_{\dot{Q}_{in}} = \dot{m}_{s30}ex_{s30} + \dot{E}x_d$
B22 (Dryer)	$\dot{m}_{s30}h_{s30} = \dot{m}_{s31}h_{s31} + \dot{m}_{s32}h_{s32}$	$\dot{m}_{s30}ex_{s30} = \dot{m}_{s31}ex_{s31} + \dot{m}_{s32}ex_{s32} + \dot{E}x_d$
Pump 2	$\dot{m}_{27}h_{27} + \dot{W}_{in} = \dot{m}_{28}h_{28}$	$\dot{m}_{27}ex_{27} + \dot{W}_{in} = \dot{m}_{28}ex_{28} + \dot{E}x_d$
Filter	$\dot{m}_{28}h_{28} = \dot{m}_{29}h_{29}$	$\dot{m}_{28}ex_{28} = \dot{m}_{29}ex_{29} + \dot{E}x_d$
3-way valve	$\dot{m}_{29}h_{29} = \dot{m}_{30}h_{30} + \dot{m}_{34}h_{34}$	$\dot{m}_{29}ex_{29} = \dot{m}_{30}ex_{30} + \dot{m}_{34}ex_{34} + \dot{E}x_d$
Throttle valve 1	$\dot{m}_{34}h_{34} = \dot{m}_{35}h_{35}$	$\dot{m}_{34}ex_{34} = \dot{m}_{35}ex_{35} + \dot{E}x_d$
Chemical treatment	$\dot{m}_{30}h_{30} = \dot{m}_{31}h_{31}$	$\dot{m}_{30}ex_{30} = \dot{m}_{31}ex_{31} + \dot{E}x_d$
Pump 3	$\dot{m}_{31}h_{31} + \dot{W}_{in} = \dot{m}_{32}h_{32}$	$\dot{m}_{31}ex_{31} + \dot{W}_{in} = \dot{m}_{32}ex_{32} + \dot{E}x_d$
RO module	$\dot{m}_{32}h_{32} = \dot{m}_{33}h_{33}$	$\dot{m}_{32}ex_{32} = \dot{m}_{33}ex_{33} + \dot{E}x_d$
Mixing chamber	$\dot{m}_{33}h_{33} = \dot{m}_{36}h_{36}$	$\dot{m}_{33}ex_{33} = \dot{m}_{36}ex_{36} + \dot{E}x_d$
Throttle valve 2	$\dot{m}_{36}h_{36} = \dot{m}_{37}h_{37}$	$\dot{m}_{36}ex_{36} = \dot{m}_{37}ex_{37} + \dot{E}x_d$

Table 6
Exergy destruction and exergy efficiency equations of components.

Component	Exergy efficiency	Exergy destruction equation
B1 (heat exchanger)	$\psi_{B1} = \frac{\dot{m}_{s2}ex_{s2} + \dot{m}_{s4}ex_{s4} + \dot{m}_{s7}ex_{s7}}{\dot{m}_{s1}ex_{s1} + \dot{m}_{s3}ex_{s3} + \dot{m}_{s10}ex_{s10}}$	$\dot{E}x_d = \dot{m}_{s1}ex_{s1} + \dot{m}_{s3}ex_{s3} + \dot{m}_{s10}ex_{s10} - (\dot{m}_{s2}ex_{s2} + \dot{m}_{s4}ex_{s4} + \dot{m}_{s7}ex_{s7})$
B3 (Gas turbine)	$\psi_{B3} = \frac{\dot{m}_{s8}ex_{s8} + \dot{W}_{out}}{\dot{m}_{s7}ex_{s7}}$	$\dot{E}x_d = \dot{m}_{s7}ex_{s7} - (\dot{m}_{s8}ex_{s8} + \dot{W}_{out})$
B4 (heat exchanger)	$\psi_{B4} = \frac{\dot{m}_{s9}ex_{s9} + \dot{m}_{s14}ex_{s14}}{\dot{m}_{s8}ex_{s8} + \dot{m}_{s14}ex_{s14}}$	$\dot{E}x_d = \dot{m}_{s8}ex_{s8} + \dot{m}_{s14}ex_{s14} - (\dot{m}_{s9}ex_{s9} + \dot{m}_{s14}ex_{s14})$
B5 (compressor)	$\psi_{B5} = \frac{\dot{m}_{s10}ex_{s10}}{\dot{m}_{s9}ex_{s9} + \dot{W}_{in}}$	$\dot{E}x_d = \dot{m}_{s9}ex_{s9} + \dot{W}_{in} - \dot{m}_{s10}ex_{s10}$
B6 (steam turbine)	$\psi_{B6} = \frac{\dot{m}_{s12}ex_{s12} + \dot{W}_{out}}{\dot{m}_{s11}ex_{s11}}$	$\dot{E}x_d = \dot{m}_{s11}ex_{s11} - (\dot{m}_{s12}ex_{s12} + \dot{W}_{out})$
B8 (pump 1)	$\psi_{88} = \frac{\dot{m}_{s14}ex_{s14}}{\dot{m}_{s13}ex_{s13} + \dot{W}_{in}}$	$\dot{E}x_d = \dot{m}_{s13}ex_{s13} + \dot{W}_{in} - \dot{m}_{s14}ex_{s14}$
B10 (heat exchanger)	$\psi_{B10} = \frac{\dot{m}_{s15}ex_{s15}}{\dot{m}_{s5}ex_{s5} + \dot{E}x_{\dot{Q}_{in}}}$	$\dot{E}x_d = \dot{m}_{s5}ex_{s5} + \dot{E}x_{\dot{Q}_{in}} - \dot{m}_{s15}ex_{s15}$
B11 (heat exchanger)	$\psi_{B11} = \frac{\dot{m}_{s21}ex_{s21}}{\dot{m}_{s6}ex_{s6} + \dot{E}x_{\dot{Q}_{in}}}$	$\dot{E}x_d = \dot{m}_{s6}ex_{s6} + \dot{E}x_{\dot{Q}_{in}} - \dot{m}_{s21}ex_{s21}$
B12 (hydrolysis reactor)	$\psi_{B12} = \frac{\dot{m}_{s16}ex_{s16}}{\dot{m}_{s15}ex_{15} + \dot{m}_{s32}ex_{32} + \dot{E}x_{\dot{Q}_{in}}}$	$\dot{E}x_d = \dot{m}_{s15}ex_{15} + \dot{m}_{s32}ex_{32} + \dot{E}x_{\dot{Q}_{in}} - \dot{m}_{s16}ex_{s16}$
B13 (separator)	$\psi_{B13} = \frac{\dot{m}_{s18}ex_{s18} + \dot{m}_{s17}ex_{s17}}{\dot{m}_{s16}ex_{s16}}$	$\dot{E}x_d = \dot{m}_{s16}ex_{s16} - (\dot{m}_{s18}ex_{s18} + \dot{m}_{s17}ex_{s17})$
B16 (decomposition reactor)	$\psi_{B16} = \frac{\dot{m}_{s22}ex_{s22}}{\dot{m}_{s21}ex_{s21} + \dot{m}_{s19}ex_{s19} + \dot{E}x_{\dot{Q}_{in}}}$	$\dot{E}x_d = \dot{m}_{s21}ex_{s21} + \dot{m}_{s19}ex_{s19} + \dot{E}x_{\dot{Q}_{in}} - \dot{m}_{s22}ex_{s22}$
B18 (heat exchanger)	$\psi_{B18} = \frac{\dot{m}_{s25}ex_{s25}}{\dot{m}_{s24}ex_{s24}}$	$\dot{E}x_d = \dot{m}_{s24}ex_{s24} - (\dot{m}_{s25}ex_{s25} + \dot{E}x_{\dot{Q}_{out}})$
B19 (electrolysis reactor)	$\psi_{B19} = \frac{\dot{m}_{s27}ex_{s27}}{\dot{m}_{s25}ex_{s25} + \dot{m}_{s26}ex_{s26} + \dot{W}_e}$	$\dot{E}x_d = \dot{m}_{s25}ex_{s25} + \dot{m}_{s26}ex_{s26} + \dot{W}_e - \dot{m}_{s27}ex_{s27}$
B20 (separator)	$\psi_{B20} = \frac{\dot{m}_{s28}ex_{s28} + \dot{m}_{s29}ex_{s29}}{\dot{m}_{s27}ex_{s27}}$	$\dot{E}x_d = \dot{m}_{s27}ex_{s27} - (\dot{m}_{s28}ex_{s28} + \dot{m}_{s29}ex_{s29})$
B21 (heat exchanger)	$\psi_{B21} = \frac{\dot{m}_{s30}ex_{s30}}{\dot{m}_{s29}ex_{s29}}$	$\dot{E}x_d = \dot{m}_{s29}ex_{s29} + \dot{E}x_{\dot{Q}_{in}} - \dot{m}_{s30}ex_{s30}$
B22 (Dryer)	$\psi_{B22} = \frac{\dot{m}_{s31}ex_{s31} + \dot{m}_{s32}ex_{s32}}{\dot{m}_{s30}ex_{s30}}$	$\dot{E}x_d = \dot{m}_{s30}ex_{s30} - (\dot{m}_{s31}ex_{s31} + \dot{m}_{s32}ex_{s32})$
Pump 2	$\psi_{pump\ 2} = \frac{\dot{m}_{28}ex_{28}}{\dot{m}_{27}ex_{27} + \dot{W}_{in}}$	$\dot{E}x_d = \dot{m}_{27}ex_{27} + \dot{W}_{in} - \dot{m}_{28}ex_{28}$
Filter	$\psi_{filter} = \frac{\dot{m}_{29}ex_{29}}{\dot{m}_{28}ex_{28}}$	$\dot{E}x_d = \dot{m}_{28}ex_{28} - \dot{m}_{29}ex_{29}$
3-way valve	$\psi_{3-way\ valve} = \frac{\dot{m}_{30}ex_{30} + \dot{m}_{34}ex_{34}}{\dot{m}_{29}ex_{29}}$	$\dot{E}x_d = \dot{m}_{29}ex_{29} - (\dot{m}_{30}ex_{30} + \dot{m}_{34}ex_{34})$
Throttle valve 1	$\psi_{TV1} = \frac{\dot{m}_{35}ex_{35}}{\dot{m}_{34}ex_{34}}$	$\dot{E}x_d = \dot{m}_{34}ex_{34} - \dot{m}_{35}ex_{35}$
Chemical treatment	$\psi_{CT} = \frac{\dot{m}_{31}ex_{31}}{\dot{m}_{30}ex_{30}}$	$\dot{E}x_d = \dot{m}_{30}ex_{30} - \dot{m}_{31}ex_{31}$
Pump 3	$\psi_{pump\ 3} = \frac{\dot{m}_{32}ex_{32}}{\dot{m}_{31}ex_{31} + \dot{W}_{in}}$	$\dot{E}x_d = \dot{m}_{31}ex_{31} + \dot{W}_{in} - \dot{m}_{32}ex_{32}$
RO module	$\psi_{RO} = \frac{\dot{m}_{33}ex_{33}}{\dot{m}_{32}ex_{32}}$	$\dot{E}x_d = \dot{m}_{32}ex_{32} - \dot{m}_{33}ex_{33}$
Mixing chamber	$\psi_{MC} = \frac{\dot{m}_{36}ex_{36}}{\dot{m}_{33}ex_{33}}$	$\dot{E}x_d = \dot{m}_{33}ex_{33} - \dot{m}_{36}ex_{36}$
Throttle valve 2	$\psi_{TV2} = \frac{\dot{m}_{37}ex_{37}}{\dot{m}_{36}ex_{36}}$	$\dot{E}x_d = \dot{m}_{36}ex_{36} - \dot{m}_{37}ex_{37}$

$$\sum_i \dot{m}_i s_i + \dot{S}_{gen} + \sum_i \left(\frac{\dot{Q}_k}{T_k}\right) = \sum_e \dot{m}_e s_e + \sum_e \left(\frac{\dot{Q}_k}{T_k}\right) \quad (5)$$

- General exergy balance equation:

$$\sum_i \dot{m}_i ex_i + \dot{E}x^Q + \dot{E}x_w = \sum_e \dot{m}_e ex_e + \dot{E}x_w + \dot{E}x^Q + \dot{E}x_d \quad (6)$$

The equations for calculating the physical and chemical exergies are expressed as follows:

$$ex_{ph} = h - h_0 - T_0(s - s_0) \quad (7)$$

$$ex_{ch} = \sum x_j ex^0_{ch} + RT_0 \sum x_j \ln(x_j) \quad (8)$$

where x_j symbolizes the mole fraction and ex^0_{ch} indicates the standard specific chemical exergy. The total exergy can be calculated as follows:

$$ex = ex_{ph} + ex_{ch} \quad (9)$$

3.1. Proton exchange membrane fuel cell (PEMFC)

The proton exchange membrane fuel cell (PEMFC) performance is calculated by:

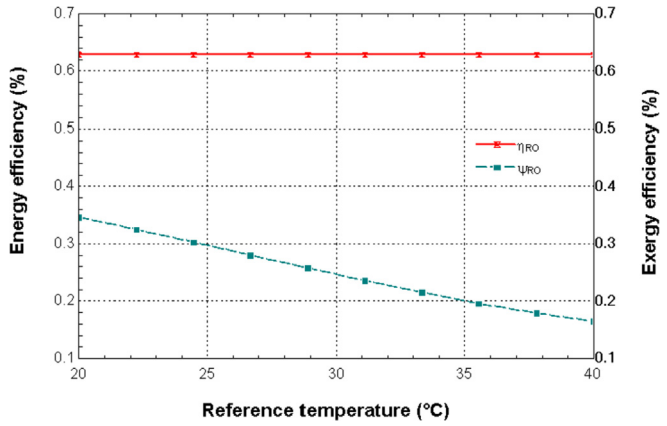

Fig. 4. Effects of reference temperature on the energy and exergy efficiency of the system.

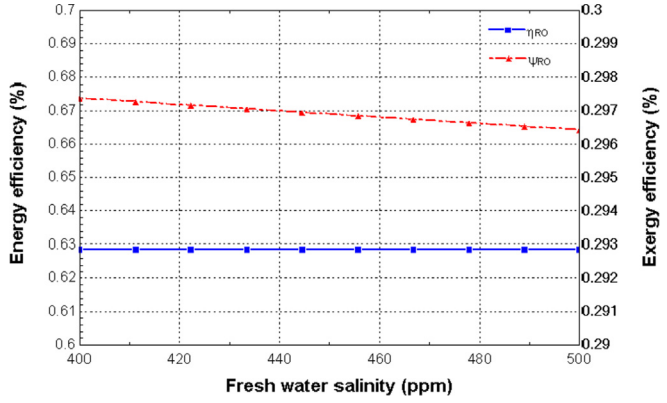

Fig. 5. Variation in the energy and exergy efficiency of the system with a change in fresh water salinity.

$$\dot{E} = \dot{E}_r - \dot{E}_{act} - \dot{E}_{Ohm} - \dot{E}_{conc} \tag{10}$$

where $\dot{E}_r$ is the reversible cell potential, $\dot{E}_{act}$ is the activation polarization, $\dot{E}_{Ohm}$ signifies ohmic polarization and P_{conc} represents concentration polarization.

The summation of cathodic and anodic activation potentials is the total activation potential and it can be expressed as:

$$\dot{E}_{act} = \dot{E}_{act,an} + \dot{E}_{act,ca} \tag{11}$$

$$\dot{E}_{act,i} = \frac{RT_{FC}}{\alpha_i nF} \ln\left(\frac{J}{J_0}\right) \tag{12}$$

where T_{FC} is fuel cell temperature, F is Faraday's constant, J is current density and α_i is the coefficient of electron transfer.

The exchange current density J_0 can be expressed as follows:

$$J_0(T) = 1.08 \times 10^{-21} \times \exp(0.086 \times T_{FC}) \tag{13}$$

The reversible cell potential can be evaluated by the Nernst equation:

$$\dot{E}_r(T, P_i) = 1.482T - 0.000845T + 4.31 \times 10^{-5} \ln\left(p_{H_2} P_{O_2}^{0.5}\right) \tag{14}$$

Here, T indicates fuel cell temperature and P denotes partial pressure.

The membrane water content λ_{mem} and membrane conductivity σ_{mem} can be expressed as:

$$\lambda_{mem} = 0.043 + 17.81a - 39.85a^2 + 39.85a^3, 0 < a \leq 1 \tag{15}$$

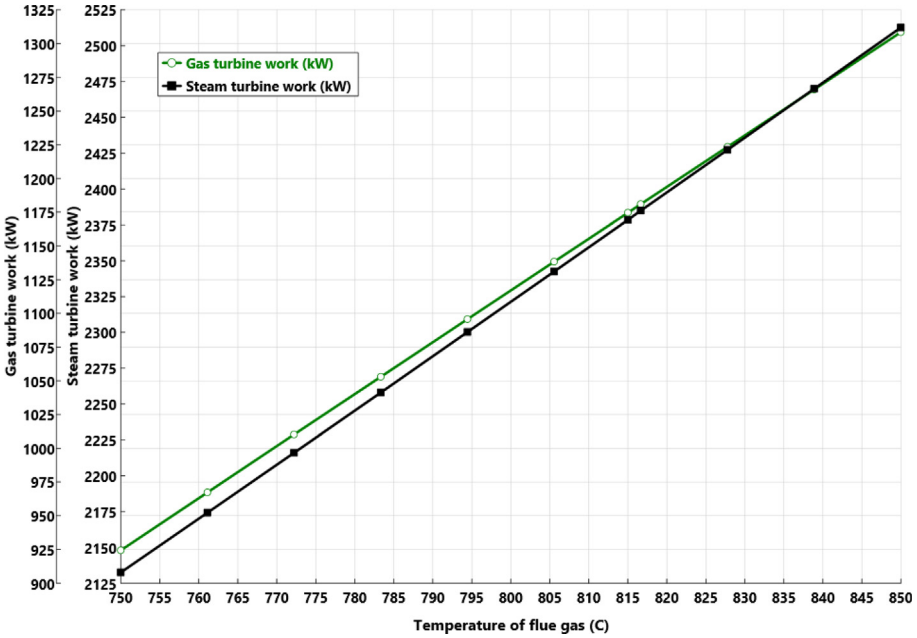

Fig. 6. Flue gas temperature effects on the gas and steam turbine power (adapted from Ref. [17]).

$$\sigma_{mem} = (0.005139\lambda_{mem} - 0.00326)\exp\left(1268\frac{1}{303} - \frac{1}{T_{FC}}\right) \quad (16)$$

The concentration polarization for the fuel cell can be written as:

$$\dot{E}_{conc} = \frac{RT}{2F}\ln\left(1 - \frac{J}{J_{L,an}}\right) + \frac{RT}{2F}\ln\left(1 + \frac{P_{H_2}J}{P_{H_2O}J_{L,an}}\right) - \frac{RT}{4F}\ln\left(1 - \frac{J}{J_{L,ca}}\right) \quad (17)$$

where $J_{L,ca}$ and $J_{L,an}$ denote the limiting current densities.

Also $\dot{Q}_{FC}$ is the heat produced by the fuel cell and the heating rate of the PEM fuel cell is 1,518 W. The power produced by an individual cell of the fuel cell is calculated by:

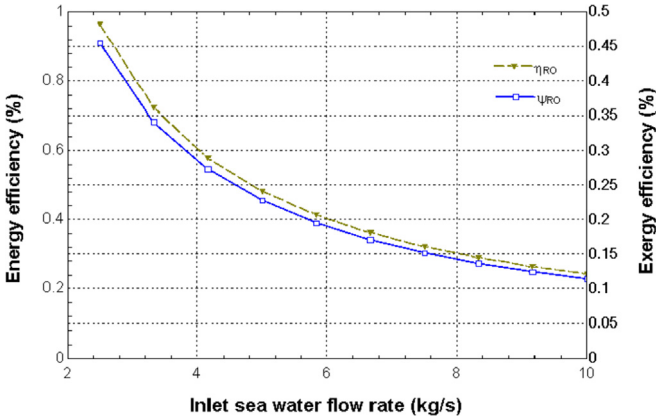

Fig. 7. Inlet sea water flow rate effects on energy and exergy efficiencies of the RO desalination unit.

$$\dot{W}_{cell} = \dot{E}(I) \times J \times A_{cell} \quad (18)$$

Here A_{cell} represents a single cell geometric area. The total stack power of the fuel cell is evaluated by multiplying the number of cells by $\dot{W}_{cell}$.

$$\dot{W}_{Stack} = n \times \dot{W}_{cell} \quad (19)$$

The fuel cell exergy destruction can be expressed by the following expression:

$$\dot{E}x_{dest,fc} = \dot{E}x_{H2} + \dot{E}x_{O2} - \dot{Q}_{fc} - \dot{W}_{stack} \quad (20)$$

3.2. Overall system efficiencies

Consider the source of heat for the system from the exhaust gas of a steel heating furnace. The overall system consists of a gas-steam combined cycle, copper-chlorine cycle, proton exchange membrane fuel cell, and reverse osmosis desalination unit. The system has four major outputs of hydrogen, electricity, fresh water and heat.

The amount of heat supplied to the copper-chlorine cycle can be expressed as follows:

$$\dot{Q}_{in} = \dot{Q}_{B1} + \dot{Q}_{B10} + \dot{Q}_{B11} + \dot{Q}_{B12} + \dot{Q}_{B14} + \dot{Q}_{B16} + \dot{Q}_{B21} \quad (21)$$

The net amount of electrical power can be expressed as:

$$\dot{W}_{net} = \dot{W}_{GT} + \dot{W}_{ST} + \dot{W}_{Stack} - \dot{W}_{compressor} - \dot{W}_{pump\ B8} - \dot{W}_e - \dot{W}_{pump2} - \dot{W}_{pump3} \quad (22)$$

The correlations for the overall energy and exergy efficiencies of the system are written as follows respectively:

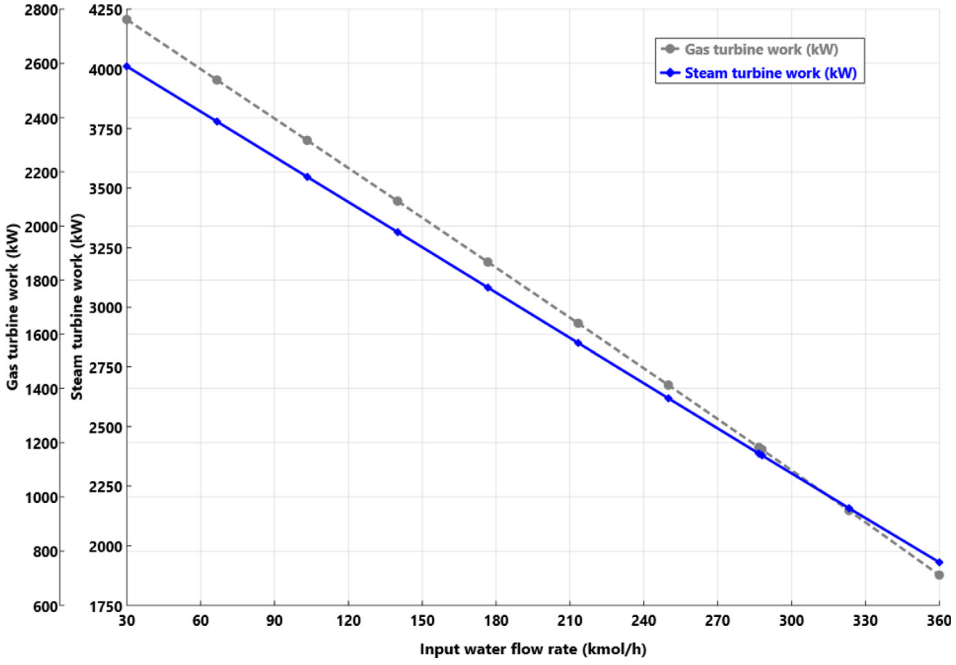

Fig. 8. Inlet water flow rate effect on gas and steam turbine power.

$$\eta_{ov} = \frac{\dot{m}_{H_2} LHV_{H_2} + \dot{W}_{net} + \dot{Q}_{FC} + \dot{m}_{fw} h_{fw}}{\dot{Q}_{in} + \dot{m}_{sw} h_{sw}} \quad (23)$$

$$\psi_{ov} = \frac{\dot{m}_{H_2} ex_{H_2} + \dot{W}_{net} + \dot{E}x_{Q_{FC}} + \dot{m}_{fw} ex_{fw}}{\dot{E}x_{\dot{Q}_{in}} + \dot{m}_{sw} ex_{sw}} \quad (24)$$

4. Results and discussion

The overall results of a case study for the multi-generation system are summarized in Table 2. Recall the operating parameters of the fuel cell like current density of the fuel cell, cell operating temperature, cell area, operating pressure of fuel cell and fuel cell heating rate were shown in Table 3.

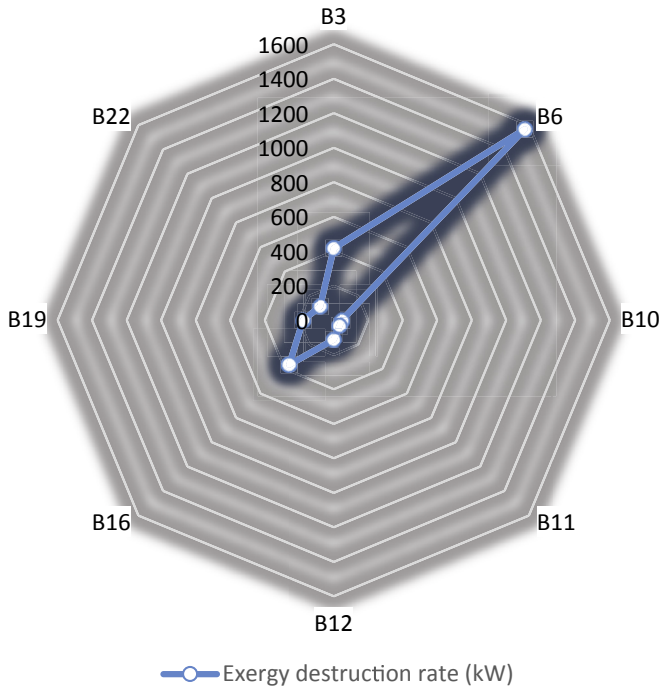

Fig. 9. Exergy destruction rates associated with significant components of the system.

Fig. 4 shows the effects of reference temperature on the energy and exergy efficiencies of the reverse osmosis desalination unit. The results show that the energy efficiency remains nearly constant with an increase in the ambient temperature while the exergy efficiency decreases at higher temperatures. The temperature change does not significantly affect enthalpies for this difference but it causes a significant variation in the exergy associated with the flow streams. With an increase in ambient temperature from 20 °C to 40 °C, the exergy efficiency declines from 35% to 17% while the energy efficiency of the system remains nearly constant at 63%.

The fresh water salinity is assumed to be 450 ppm. The effects of salinity on the energy and exergy efficiencies of the RO desalination system are shown in Fig. 5. The results show that the energy efficiency does not change significantly with fresh water salinity but the exergy efficiency of the system decreases slightly with an increase in salinity. The energy efficiency almost remains constant at 62.9% while the exergy efficiency decreases slightly from 29.8% to 29.6% in the figure.

Table 4 presents significant parameters such as the salinity of sea water, salinity of product water, fresh water flow rate, sea water temperature, pump efficiency and membrane recovery ratio for the reverse osmosis desalination unit.

The effects of flue gas temperature on the system parameters are seen in Fig. 6. The graph shows the effect of flue gas temperature on the power produced by the gas and steam turbines. For an increase in temperature of the flue gas, the power produced by the gas and steam turbine increases. If the temperature increases from 810 °C to 850 °C, the gas turbine work will increase from 1,174 kW to 1,350 kW while the power produced by the steam turbine will increase from 2,378 kW to 2,500 kW.

The effect of sea water inlet flow rate on the energy and exergy efficiencies of the system is illustrated in Fig. 7. It is observed that with an increase in inlet sea water flow rate, the energy and exergy efficiencies of the desalination system decrease. The figure shows that the energy and exergy efficiencies of the system decrease from 91% to 12% with an increase in sea water flow rate from 2 kg/s to

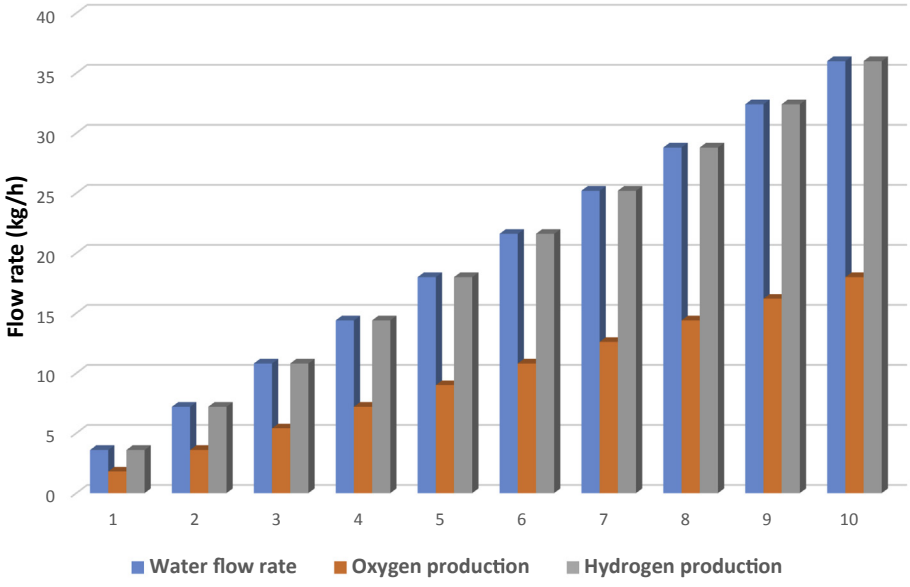

Fig. 10. Effects of water flow rate on hydrogen and oxygen production rates.

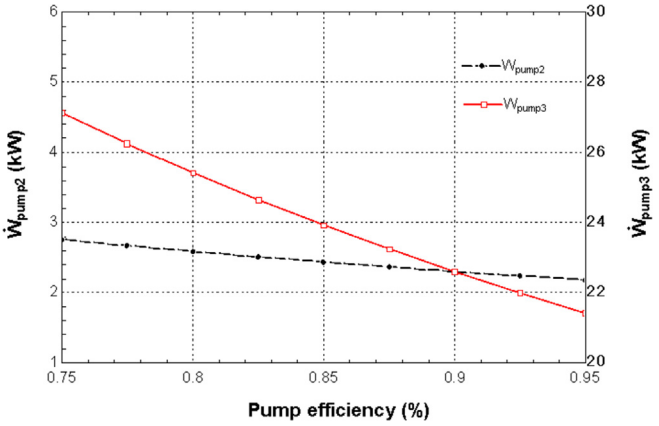

Fig. 11. Effects of varying pump isentropic efficiency on power consumption.

10 kg/s.

The inlet water flow rate effects on the gas and steam turbine power are shown in Fig. 8. With an increase in the input water flow rate associated with the stream S3, the power produced by the gas and steam turbine decrease at the same time. The thermal energy linked with the stream S3 increases which results in decreasing the thermal energy supplied to the gas-steam combined cycle and eventually this leads to reduced power generation.

The exergy destruction rates associated with the major components of the system are shown in Fig. 9. The maximum exergy destruction rate is associated with the steam turbine, while the second highest exergy destruction rate is carried by the gas turbine, while the third highest exergy destruction rate is observed with the decomposition reactor. The graphical representation shows the dot in the direction of the component names from the vertex.

Fig. 10 illustrates the effects of the flow rate of water on hydrogen and oxygen production. Water is the only input component in the copper-chlorine cycle while all remaining components like cuprous chloride, copper oxychloride, hydrogen chlorine and cupric chloride are recycled within the system. Thus, Fig. 10 shows that with an increase in water flow rate, the hydrogen and oxygen production rates increase as expected.

Fig. 11 illustrates the effects of the pump isentropic efficiency on the work consumption. If the pump efficiency is reduced, pumps will consume more power while if the pump efficiency is increased, the power consumption by low pressure and high pressure pumps can be decreased.

5. Conclusions

Thermal management of steel furnace waste heat was analyzed in this paper. The system consists of a gas-steam combined cycle, thermochemical copper-chlorine (Cu–Cl) cycle, proton exchange membrane fuel cell and a reverse osmosis desalination unit. Additional heat recovered from the steelmaking process is employed in a gas-steam combined cycle in order to generate more power. This paper has examined the effect of the combined cycle on the system performance and effects of the temperature of the condenser to produce fresh water via an RO desalination unit. A significant portion of the heat recovered is utilized in the copper-chlorine (Cu–Cl) cycle. Oxygen produced by the Cu–Cl cycle and a partial amount of hydrogen is consumed in the PEM electrolyzer to generate heat and electricity. The system is based on multi-outputs of hydrogen, electricity, fresh water and heat. The overall hydrogen production rate of the system is 51.8 kg/hr and the net power production is 1.7 MW. A reverse osmosis desalination unit produces 2.3 kg/s of fresh water which is sufficient for a community of about 200 households. Electric power produced by the proton exchange membrane fuel cell is 13.8 kW. The overall energy and exergy efficiencies of the integrated system are 63.3% and 58.8% respectively.

Nomenclature

A	area (m^2)
$\dot{E}n$	energy rate (kW)
ex	specific exergy (kJ/kg)
$\dot{E}x$	exergy rate (kW)
$\dot{E}x_{dest}$	exergy destruction (kW)
h	specific enthalpy (kJ/kg)
LLV	lower heating value (kJ/kg)
$\dot{m}$	mass flow rate (kg/s)
n	number of moles
P	pressure (kPa)
Q	heat (kJ)
$\dot{Q}$	heat rate (kW)
R	gas constant (kJ/kmol K)
s	specific entropy (kJ/kg K)
$\dot{S}_{gen}$	Entropy generation rate (kW/K)
T	temperature (°C)
V	Volume
$\dot{W}$	Power or work rate (kW)

Greek letters

η	energy efficiency
ψ	exergy efficiency

Subscripts

0	ambient conditions
B#	block name in Aspen Plus
CC	combined cycle
Comp	compressor
ch	chemical
en	energy
ex	exergy
H_2	hydrogen
i	input
ov	overall
O_2	oxygen
p	pump
RO	reverse osmosis
W	work

Acronyms

Cu–Cl	Copper–Chlorine cycle
EAF	Electric Arc Furnace
EES	Engineering Equation Solver
GT	Gas Turbine
HEX	Heat Exchanger
ST	Steam Turbine

References

[1] Ishaq H, Dincer I, Naterer GF. Performance investigation of an integrated wind energy system for co-generation of power and hydrogen. Int J Hydrogen Energy 2018;43:9153–64.
[2] Naterer GF, Dincer I, Zamfirescu C. Hydrogen production from nuclear energy. London New York: Springer Verlag; 2013. https://doi.org/10.1007/978-1-4471-4938-5.
[3] Dincer I, Rosen M. Thermal energy storage systems and applications. Hoboken, New Jersey: Wiley; 2003.
[4] Dincer I, Colpan CO, Kizilkan O, Ezan MA. Progress in clean energy. Novel

systems and applications, vol. 2. Springer; 2015.
[5] Naterer GF, Dincer I, Zamfirescu C. Hydrogen production from nuclear energy. London, New York: Springer; 2013.
[6] Naterer GF, Suppiah S, Stolberg L, Lewis M, Wang Z, Rosen MA, Dincer I, Gabriel K, Odukoya A, Secnik E, Easton EB, Papangelakis V. Progress in thermochemical hydrogen production with the copper-chlorine cycle. Int J Hydrogen Energy 2015;40:6283–95.
[7] Szargut J. Influence of regenerative feed water heaters on the operational costs of steam power plants and HP plants. Int J Therm 2005;8:137–41.
[8] Wang Z, Naterer GF, Gabriel KS, Secnik E, Gravelsins R, Daggupati V. Thermal design of a solar hydrogen plant with a copper-chlorine cycle and molten salt energy storage. Int J Hydrogen Energy 2011;36:11258–72.
[9] Szargut JT. Optimization of the design parameters aiming at the minimization of the depletion of non-renewable resources. Energy 2004;29:2161–9.
[10] Liang X, Pan G, Xu L, Wang J. A modified decal method for preparing the membrane electrode assembly of proton exchange membrane fuel cells. Fuel 2015;139:393–400.
[11] Szargut J, Szczygiel I. Comparison of the efficiency of the variants of a primary gas turbine supplementing a coal-fired power plant. Energy 2005;30:1204–17.
[12] Gantenberg M, Eschmann F, El-Kassas H. Waste gas heat recovery system - technology and economic experiences to reduce the operating expenditures of a blast furnace shop. In: AISTech - Iron Steel Technol. Conf. Proc. I; 2011. p. 551–61.
[13] Si M. The feasibility of waste heat recovery and energy efficiency assessment in a steel plant. 2011.
[14] Szargut J, Szczygiel I. Utilization of the cryogenic exergy of liquid natural gas (LNG) for the production of electricity. Energy 2009;34:827–37.
[15] Szargut J. Influence of the ambient temperature on the operational indices of the gas turbine set. Int J Energy Res 2000;24:821–30.
[16] Naterer GF, Suppiah S, Stolberg L, Lewis M, Wang Z, Rosen MA, Dincer I, Gabriel K, Odukoya A, Secnik E, Easton EB, Papangelakis V. Progress in thermochemical hydrogen production with the copper-chlorine cycle. Int J Hydrogen Energy 2015;40:6283–95.
[17] Ishaq H, Dincer I, Naterer GF. Industrial heat recovery from a steel furnace for the cogeneration of electricity and hydrogen with the copper-chlorine cycle. Energy Convers Manag 2018;171:384–97.
[18] Siddiqui O, Dincer I. A review and comparative assessment of direct ammonia fuel cells. Therm Sci Eng Prog 2018;5:568–78.
[19] Khalid F, Dincer I, Rosen MA. Analysis and assessment of a gas turbine-modular helium reactor for nuclear desalination. J Nucl Eng Radiat Sci 2016;2:31014.
[20] Almahdi M. Integrated heat pump options for heat upgrading in Cu-Cl cycle for hydrogen production. 2016.
[21] Nguyen-Schäfer H. Rotordynamics of automotive turbochargers. Springer; 2012.
[22] Al-Zareer M, Dincer I, Rosen MA. Development of an integrated system for electricity and hydrogen production from coal and water utilizing a novel chemical hydrogen storage technology. Fuel Process Technol 2017;167:608–21.
[23] Al-Zareer M. Conceptual development and analysis of multiple integrated hydrogen production plants with Cu-Cl cycle. 2016.
[24] Ozbilen AZ. Development, analysis and life cycle assessment of integrated systems for hydrogen production based on the copper-chlorine (Cu-Cl) cycle. Univ. Ontario Inst; 2013. https://doi.org/10.1073/pnas.0703993104. Technol.: PhD Thesis.
[25] Islam S, Dincer I, Yilbas BS. Development of a novel solar-based integrated system for desalination with heat recovery. Appl Therm Eng 2018;129:1618–33.
[26] Cengel YA, Boles MA. Thermodynamics: an engineering approach. eighth ed. McGraw-Hill; 2015. https://doi.org/10.1017/CBO9781107415324.004.
[27] Dincer I, Rosen MA. Exergy: energy, environment and sustainable development. Amsterdam, Netherlands: Elsevier; 2013.